Egypt. J. Phys. **Vol. 53,** pp. 21-42 (2025)

Egyptian Journal of Physics

https://ejphysics.journals.ekb.eg/

Boson Stars with U(1) Symmetric Potentials as Candidates for Black Hole Mimickers

Mahmoud Rezk [2], Fawzy S. Tarabia [1] and Muhammad Maher[1]

[1] *Physics Department, Faculty of Science, Helwan University, 11792 Ain Helwan, Cairo, Egypt.*

[2] *Basic Sciences Department, Faculty of Engineering, Modern University for Technology and Information (MTI), 11571 Cairo, Egypt.*

Abstract

WE study the configurations of a spherically symmetric boson star (BS) models with different general self-interaction terms of U(1) symmetry type. We modify these potentials to include only one rescaled dimensionless decay constant as a single control parameter, which results in a small change in the BS configuration, particularly in the star's maximum mass. We then study these BS configurations in terms of a simple accretion disc model spiraling around the boson star. Through the comparative study of the power spectrum (luminosity) at different values of the decay constants of the different boson star configurations studied corresponding to the different potentials involved in the present study, we found a unique boson star configuration that mimics a particular black hole (BH) configuration for each potential at a given decay constant value. Finally, we lay a blueprint for matching the currently observed gravitational wave signals with the maximum masses of the boson star mimickers we obtained.

Keywords: boson stars, compact objects, black holes, general relativity, scalar fields, Einstein-Klein-Gordon equations.

Introduction

Due to several discoveries of high energy events, the nature of black hole candidates or 'mimickers' is currently a significant issue in relativistic astrophysics. There has been some interest in the subject of whether black hole mimickers are just ordinary black hole solutions or something else.

Historically, It was first discussed as particle-like object by Wheeler to construct solutions for classical fields of electromagnetic–real scalar field–coupled to gravity [15, 23] to be able to describe what he called "gravitational atom" he called the solutions to his system "geons" and they were unstable.

Then Kaup [11] replaced electromagnetic fields with a system of complex scalar field; Klein-Gordon "geons". This system was the core of boson star model(s) used in this paper.

Compared to most other classes of potentially compact objects, boson star (BS) models have great advantage because the equations describing them are relatively simple unlike other widely used neutron or fermion star models, for instance. Boson star models do not obey Pauli Exclusion Principle but obey Heisenberg Uncertainty Principle. Accordingly, bosons are being localized in their Compton wavelength causing the star to avoid collapsing to form a black hole.

*Corresponding author: Muhammad Maher, E-mail: m.maher@science.helwan.edu.eg.
Received: 18 January 2025, Accepted: 24 Febraury2025
DOI: 10.21608/ejphysics.2025.353879.1105

As we will discuss in more depth in the next section, there exists variants of boson star models with different potentials. The simplest BS model, which is widely considered as a toy model for verifying and calibrating numerical solutions is the so-called mini-boson star model, which was first introduced by Kaup [11]. The study of nonlinear potentials in the context of BS modeling was first explored numerically by Mielke and Scherzer [14]. Later, it was shown by Colpi, Shapiro, and Wasserman that because of the quartic self-interaction potential in boson Lagrangian, the BS system could yield higher values for maximum mass compared with the non-interacting equivalent [3].

More studies on nonlinear potentials were performed by Schunck and Torres [18] who discussed potentials that yield different BS maximum mass values, which can be related to some observable signals that can be used to detect BSs as we are going to explain in more detail in section (3.2).

To stress the novelty of the present work at this early stage of our layout, we highlight the following:

- We extend the discussion in ref. [18] to investigate the possibility that boson star models with different nonlinear unitary potentials can mimic black holes.
- Unlike the approach used in ref. [18], we reformulate the potentials used to ensure they depend on a single decay constant and that they are properly rescaled to be dimensionless.
- In this vein, we exploit the simple accretion disc model and the associated power spectrum discussed in refs. [7, 21].
- Unlike the efforts reported in refs. [7, 21] using a single-type of nonlinear potentials, we implement here three different types of nonlinear potentials in the calculation of the power spectrum. We have also used the mini-boson star potential as a toy model to initially calibrate our numerical code and also as reference non-interacting BS system.
- We lay down some blueprint to link our calculations of the BS maximum masses to some observable gravitational wave (GW) signals.

This paper is organized as follows: in Sec. 2, the Einstein-Klein-Gordon (EKG) equations, which govern the behaviour of scalar fields and gravity, are outlined. Then we rescale the EKG equations to ensure they are dimensionless. We then modify the potentials to guarantee their dependence on only one free parameter, namely the rescaled decay constant. Finally numerical results for the model at different potentials are obtained at two different values of the rescaled decay constant.

In Sec. 3, we determine the luminosity for both the BS system and the corresponding BH at maximum BS mass. We then fix the BS configuration that can mimic the BH luminosity profile. We terminate Sec. 3 with a discussion of the observational challenges relevant to the present work, and we introduce some GW signal based detection scenario. We finally summarize the present work and conclude in Sec. 4.

Before getting any deeper, we need to alert the reader that we use throughout this paper a unit convention in which $\hbar = 1$, $m_p = \frac{1}{\sqrt{G_N}}$, and $M_p = \frac{1}{\sqrt{8\pi G_N}}$.

<u>Boson star Model</u>

We start with the following action

$$S = \int d^4 x\sqrt{-g}\left(\frac{R}{16\pi G_N}\mathcal{L}\right). \qquad (1)$$

The corresponding Lagrangian density is

$$\mathcal{L} = -\frac{R}{16\pi} + g^{\mu\nu}\,\partial_\mu\phi^*\,\partial_\nu\phi + V(|\phi|^2) \qquad (2)$$

, where R: Ricci scalar, $g^{\mu\nu}$: Metric function,

ϕ: Scalar field, V: Potential of the scalar field,

$\sqrt{-g}$: Determinant of the metric.

When the action is varied with respect to the metric it gives Einstein equation which reads

$$G_{\mu\nu} = 8\pi T_{\mu\nu}\ , \qquad (3)$$

where $G_{\mu\nu}$ is Einstein tensor and $T_{\mu\nu}$ is the momentum- energy tensor which is given based on equation (2) in the form

$$T_{\mu\nu} = \frac{1}{2}\left(\partial_\mu\phi^* \partial_\nu\phi + \partial_\mu\phi\, \partial_\nu\phi^*\right) - \frac{1}{2}g_{\mu\nu}\left(\phi^{*,a}\phi_{,a} + V(|\phi|^2)\right). \quad (4)$$

The variation of equation (1) with respect to the scalar field ϕ gives Klein Gordon equation

$$\left(\Box - \frac{dV}{d|\phi|^2}\right)\phi = 0, \quad (5)$$

where $\Box\,\phi = \frac{1}{\sqrt{-g}}\partial_\mu\left[\sqrt{-g}g^{\mu\nu}\,\partial_\nu\phi\right]$.

To ensure time-invariance of the square of the scalar field, we choose a scalar field ϕ of the form:

$$\phi(r,t) = \phi_0 e^{-i\omega t}\ , \quad (6)$$

where ω is the angular frequency. Note that it must be real number and also choosing this form for the scalar field in the previous equation makes the momentum-energy tensor time independent. Since we want deal with spherical symmetric boson star model(s), we use the following line element:

$$ds^2 = -\alpha^2 dt^2 + a^2 dr^2 + r^2 d\Omega^2 \quad (7)$$

, where $\alpha(r)$ and $a(r)$ are lapse and radial functions in r, respectively. From equations (3) and (5) with line element (7) and using the same derivation procedures as in refs. [4, 6, 7], we construct our EKG system of equations as follows:

$$\frac{\partial a}{\partial r} = a\left[\frac{1-a^2}{2r} + \frac{1}{4}\kappa r G_N\left(\omega^2\phi^2\frac{a^2}{\alpha^2} + \Phi^2 + a^2 V(|\phi|^2)\right)\right] \quad (8a)$$

$$\frac{\partial \alpha}{\partial r} = \alpha\left[\frac{a^2-1}{2r} + \frac{1}{4}\kappa r G_N\left(\omega^2\phi^2\frac{a^2}{\alpha^2} + \Phi^2 - a^2 V(|\phi|^2)\right)\right] \quad (8b)$$

$$\frac{\partial^2\phi}{\partial r^2} = -\left[\frac{2}{r} + \left(\frac{\partial\alpha}{\partial r}\frac{1}{\alpha}\right) - \left(\frac{\partial a}{\partial r}\frac{1}{a}\right)\right] - \omega^2\phi\frac{a^2}{\alpha^2} + a^2\frac{dV}{d|\phi|^2} \quad (8c)$$

, where $\kappa = 8\pi$. Note that in left hand side of (8c), ϕ has a second derivative in r. Thus, to make all the constituent equations of the system (8) have first derivative in r, we introduce a new variable Φ such that $\frac{\partial\phi}{\partial r} = \Phi$, then we obtain the following update:

$$\frac{\partial a}{\partial r} = a\left[\frac{1-a^2}{2r} + \frac{1}{4}\kappa r G_N\left(\omega^2\phi^2\frac{a^2}{\alpha^2} + \Phi^2 + a^2 V(|\phi|^2)\right)\right] \quad (9a)$$

$$\frac{\partial \alpha}{\partial r} = \alpha\left[\frac{a^2-1}{2r} + \frac{1}{4}\kappa r G_N\left(\omega^2\phi^2\frac{a^2}{\alpha^2} + \Phi^2 - a^2 V(|\phi|^2)\right)\right] \quad (9b)$$

$$\frac{\partial\phi}{\partial r} = \Phi \quad (9c)$$

$$\frac{\partial\Phi}{\partial r} = -\left[\frac{2}{r} + \left(\frac{\partial\alpha}{\partial r}\frac{1}{\alpha}\right) - \left(\frac{\partial a}{\partial r}\frac{1}{a}\right)\right] - \omega^2\phi\frac{a^2}{\alpha^2} + a^2\frac{dV}{d|\phi|^2} \quad (9d)$$

We then rescale the system of equations (9) to ensure that system is dimensionless keeping in mind that $V(|\phi|^2)$ has dimension of $[Energy]^4$. We rescale the following variables in this manner $\tilde{r} = r m_\phi$, $\tilde{\omega} = \omega/m_\phi$, $\left(\tilde{\phi}\right)^2 = 8\pi G_N\phi^2$ $\tilde{V} = \left(8\pi G_N/m_\phi^2\right)V$

$$\frac{\partial\tilde{a}}{\partial\tilde{r}} = \tilde{a}\left[\frac{1-\widetilde{a^2}}{2\tilde{r}} + \frac{1}{4}\kappa\tilde{r}\left((\tilde{\omega})^2\left(\tilde{\phi}\right)^2\frac{(\tilde{a})^2}{(\tilde{\alpha})^2} + \tilde{\Phi} + (\tilde{a})^2\tilde{V}\right)\right] \quad (10a)$$

$$\frac{\partial\tilde{\alpha}}{\partial\tilde{r}} = \tilde{\alpha}\left[\frac{1-(\tilde{a})^2}{2\tilde{r}} + \frac{1}{4}\kappa\tilde{r}\left((\tilde{\omega})^2\left(\tilde{\phi}\right)^2\frac{(\tilde{a})^2}{(\tilde{\alpha})^2} + \tilde{\Phi} - (\tilde{a})^2\tilde{V}\right)\right] \quad (10b)$$

$$\frac{\partial\tilde{\phi}}{\partial\tilde{r}} = \tilde{\Phi} \tag{10c}$$

$$\frac{\partial\tilde{\Phi}}{\partial\tilde{r}} = -\left[\frac{2}{\tilde{r}} + \left(\frac{\partial\tilde{\alpha}}{\partial\tilde{r}}\cdot\frac{1}{\tilde{\alpha}}\right) - \left(\frac{\partial\tilde{a}}{\partial\tilde{r}}\cdot\frac{1}{\tilde{a}}\right)\right] - (\tilde{\omega})^2(\tilde{\phi})^2\frac{(\tilde{a})^2}{(\tilde{\alpha})^2} + (\tilde{a})^2\frac{d\tilde{V}}{d|\tilde{\phi}|^2}\tilde{\phi}\,. \tag{10d}$$

Since the action equation (1) has global invariance under U(1) symmetry for scalar field $\phi \to e^{i\theta}$, then it implies that there is Noether current

$$J^\mu = ig^{\mu\nu}(\phi^\star\partial_\nu\phi - \phi\partial_\nu\phi^\star) \tag{11}$$

Since Noether current gives the total number of particles [16]

$$N = \int d^3\,x\sqrt{-g}J^0. \tag{12}$$

As we can see from the system of equations (10), it is a system of ordinary differential equation with unknown variable $\tilde{\omega}$. We numerically solve the system (10) using Runge-Kutta fourth order method, and then we perform a binary search for a particular $\tilde{\omega}$ value that meets our acceptable tolerance for all variables in the system of equations (10).

Lastly we calculate the mass of the boson star using Misner-Sharp mass (ADM formalism) which is calculated through metric functions as prescribed in ref. [1].

$$M(r) = (1 - 1/a^2)r^2 \tag{13}$$

2.1. Self-interaction potentials

The most basic boson star model is the mini-boson star that was first introduced in [11] and [16]. According to [14], the non-linear expansion for the self-interacting potentials may have the generic form

$$V(|\phi|^2)_{nonlinear} = m^2|\phi|^2 - \lambda_1\phi^4 + \lambda_2|\phi|^6. \tag{14}$$

If we choose the prescription outlined in [3], we also have the choice of writing the non-linear expansion for the potential in the form

$$V(|\phi|^2)_{quartic} = m^2|\phi|^2 + \frac{\lambda|\phi|^4}{2}. \tag{15}$$

Rescaling (15) using $\Lambda = \lambda M_p^2/m_\phi^2$, we obtain

$$V(|\phi|^2)_{quartic} \times \left(8\pi G_N/m_\phi^2\right) = \left|\tilde{\phi}\right|^2 + \frac{\Lambda\left|\tilde{\phi}\right|^4}{2}. \tag{16}$$

As a toy model for calibrating our numerical code, we use the rescaled mini-boson star potential given in eqn. (16) with $\Lambda = 0$. In this case, the mass scales as $\sim M_{pl}^2/m_\phi$. Note also that when $\Lambda \neq 0$, the mass $M \sim M_{pl}^3/m_\phi^2$, which is roughly close to Chandrasekhar mass given by $M \sim M_{pl}^3/m_n^2$, which is close to mass of the sun, where m_n is the neutron mass.

The potentials described above are considered to be by repulsive potentials, which imply that they support the bosonic quantum pressure arising from the uncertainty principle and opposing the gravitational attractive force that tends to collapse the star.

Moreover, we also consider the potentials discussed in [18] in the context of our search for possible candidates for a black hole mimickers. The idea is to examine the possibility if a series of repulsive or repulsive and attractive bosonic self-interaction terms producing some maximum BS mass and compactness that makes those BS configurations observationally comparable with some supermassive black hole with a typical astronomically relevant mass in the order of $10^9 M_\odot$. Supermassive black holes of that mass are predicted to exist at the canter of massive galaxies such as M87 as well as quasars such as 3C 273 [26]. The comparison is planned to primarily rely on the comparative fitting of the luminous accretion rate of the disc model data.

The first potential that we are going to consider here is the Cosh-Gordon which comes in the form

$$V_{cosh} = \alpha m^2\left(\cosh\left(\beta\sqrt{|\phi|^2}\right) - 1\right) \tag{17}$$

Note in last equation there are two free parameters, namely α and β, which we will reduce to only one free parameter, namely f, by expanding equation (17) as follows

$$V_{cosh} = \alpha m^2(\cosh(\beta\phi) - 1) = \alpha m^2\left(\frac{\beta^2\phi^2}{2} + \frac{\beta^4\phi^4}{24} + \frac{\beta^6\phi^6}{720} + \cdots\right) \tag{18}$$

From last equation we can reintroduce (17) by replacing α and β by f. This yields

$$V_{cosh} = 2m^2f^2\left(\cosh\left(\frac{\sqrt{|\phi|^2}}{f}\right) - 1\right). \tag{19}$$

We then use the same algorithm for modifying our potentials. The next potential to consider here is the "sin-Gordon" which comes in the following form

$$V_{sin} = \alpha m^2\left(\sin\left(\pi/2\left(\beta\sqrt{|\phi|^2}\right)\right) + 1\right). \tag{20}$$

Expanding (20) we obtain

$$V_{sin} = \alpha m^2\left(\sin\left(\pi/2(\beta\phi - 1)\right) + 1\right) = \alpha m^2\left(\frac{\beta^2\pi^2\phi^2}{8} - \frac{\beta^4\pi^4\phi^4}{384} + \frac{\beta^6\pi^6\phi^6}{46080} + \cdots\right). \tag{21}$$

We then replace α such that $\alpha = \frac{8}{\pi^2}\frac{1}{\beta^2} = \frac{8}{\pi^2}f^2$ in the above expansion. Equation (20) thus becomes

$$V_{sin} = \frac{8}{\pi^2}f^2m^2\left(\sin\left(\pi/2\left(\frac{\sqrt{|\phi|^2}}{f}\right)\right) + 1\right). \tag{22}$$

We finally do the same procedure for the "Liouville potential" of the form

$$V_{Lio} = \alpha m^2(\exp(\beta^2|\phi|^2) - 1). \tag{23}$$

Its expansion comes in the following form

$$V_{Lio} = \alpha m^2(\exp(\beta^2\phi^2) - 1) = \alpha m^2\left(\beta^2\phi^2 + \frac{\beta^4\phi^4}{2} + \frac{\beta^6\phi^6}{6} + \cdots\right). \tag{24}$$

From the above expansion, we can again replace α and β by f to obtain

$$V_{Lio} = f^2m^2\left(\exp\left(\frac{|\phi|^2}{f^2}\right) - 1\right). \tag{25}$$

We must point out here before moving forward with the potential rescaling process that all expansions depicted equations (18), (21), and (24) have the mass term scales with (m^2), which is important to give scalar field solutions that decrease exponentially with the scalar field (ϕ) to ensure the finiteness of spacial extent of the field. We also note that the cosh-Gordon and the Liouville-Gordon potentials are a series of repulsive potentials and the sin-Gordon is series of attractive and repulsive potentials. By modifying these potentials such that they depend on a single parameter; the decay constant, we make it easier to make better control on our numeric and thereby easier to compare with black hole parameters in search for candidate mimickers.

Now it's time to rescale the potentials under consideration to make them dimensionless. We follow the same technique we used in rescaling equation (16).

Sin-Gordon potential:

$$V_{sin} \times \left(8\pi G_N/m_\phi^2\right) = \frac{8}{\pi^2}\left(\tilde{f}\right)^2\left(\sin\left(\pi/2\left(\frac{\sqrt{|\tilde{\phi}|^2}}{\tilde{f}}\right)\right) + 1\right) \tag{26}$$

Cosh-Gordon potential:

$$V_{cosh} \times \left(8\pi G_N/m_\phi^2\right) = 2\left(\tilde{f}\right)^2\left(\cosh\left(\frac{\sqrt{|\tilde{\phi}|^2}}{\tilde{f}}\right) - 1\right) \tag{27}$$

Liouville potential:

$$V_{lio} \times \left(8\pi G_N/m_\Phi^2\right) = \left(\tilde{f}\right)^2 \left(\exp\left(\frac{|\tilde{\phi}|^2}{\left(\tilde{f}\right)^2}\right) - 1\right) \tag{28}$$

The (rescaled) potential forms (26-28) all have $\left(\tilde{f}\right)^2 = 8\pi G_N f^2$. These forms are the ones we plug in the system of equations (10), one at a time during our numerical calculations leading to the numerical results to be presented in the next section.

2.2. Results and Analysis

In this section we present equilibrium solutions for the system of equations (10). Remember that these equations are of dimensionless form.

As a boundary condition, we must ensure asymptotic flatness for the outer boundary. Thus, we require that

$(\alpha(\tilde{r} \to \infty) = 1/a(\tilde{r} \to \infty) = \phi(\tilde{r} \to \infty) = 0)$.

Similarly, to ensure regularity at the inner boundary, we require that

$(\alpha(0) = 1/a(0), \phi(0) = \phi_0, \phi'(0) = 0)$.

Now it is apparent that the only unknown variable remaining in the set of equations (10) is $(\tilde{\omega})$ which reduces our problem to an eigenvalue problem. In the equation set (10), for each value of $\tilde{\phi}$ at $\tilde{r} = 0$ is associated with a unique value of $\tilde{\omega}$ that exponentially grows with the value of $\tilde{\phi}$. In our numerical solution, we use the shooting method to predict the value of $\tilde{\omega}$. Since our system of equations (10) either diverges in the upper or the lower bound, we were able to perform a binary search to predict the value of $\tilde{\omega}$. We do that by assuming we have a range between the lower and the upper bounds $\left[\widetilde{\omega_\iota}, \widetilde{\omega_f}\right]$ that contains our desired value within.

We then test the midpoint by solving the system of equations (10) and finally we check for divergence from this middle point. Based on this test, we modify the lower and upper bounds of $\left[\widetilde{\omega_\iota}, \widetilde{\omega_f}\right]$ till we end up with a very small range within which our desired value of $\tilde{\omega}$ lies. As a test of this method, it is applied to the simplest BS model; the mini-boson star. We found that our solution exactly matches the maximum mass viewed of the mini-boson star at all points. These results are listed in Table (1). In the present paper, we don't explicitly study the stability of our model(s), which we prefer to study elsewhere. However, the interested reader is advised to read some other BS stability treatments, for example [4], [5], [6] for an analytical approach, and [19], [8], [12] for a numerical one.

As we can see from figures (1-7), the radial profiles for different potentials are the same due to the form equation (10c), and this functional form is due to the initial value of ϕ_0 and potential form.

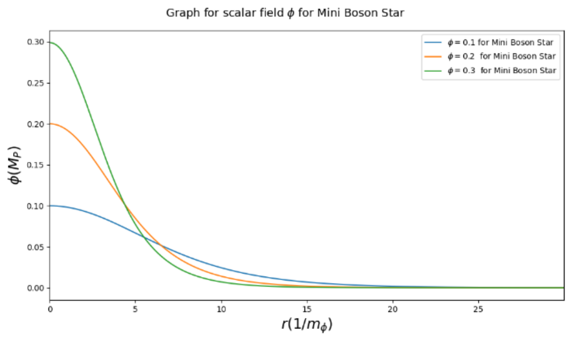

Fig. 1: Scalar field for mini boson star $\Lambda = 0$

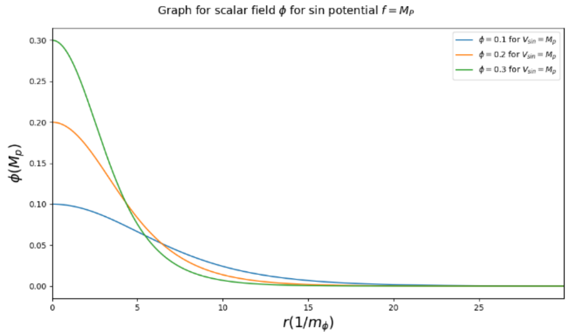

Fig. 2: Scalar field for sine potential $f = M_p$

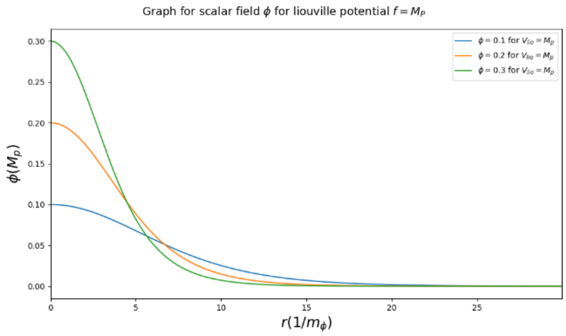

Fig. 3: Scalar field for Liouville potential $f = M_p$

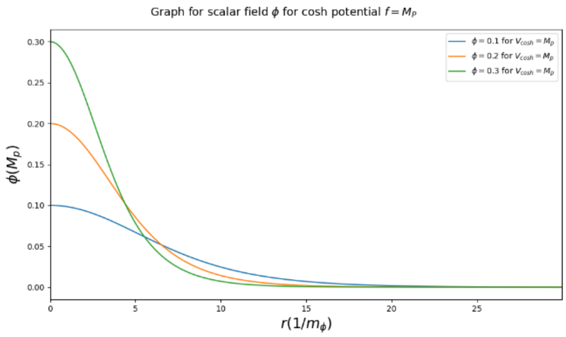

Fig.4: Scalar field for cosh potential at $f = M_p$

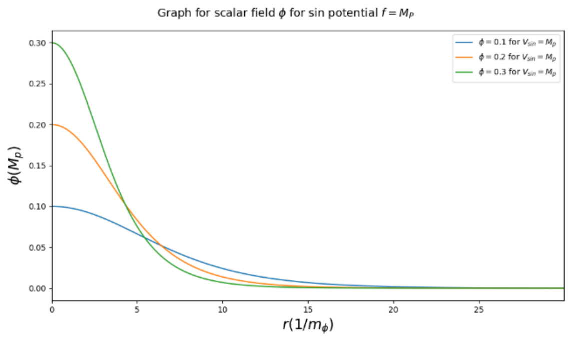

Fig.5: Scalar field for sine potential at $f = 0.9M_p$

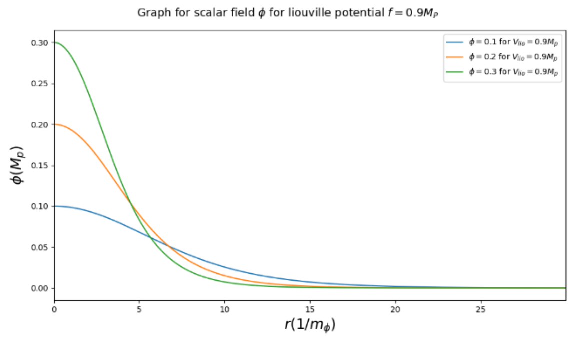

Fig.6: Scalar field for Liouville potential at $f\, = 0.9M_p$

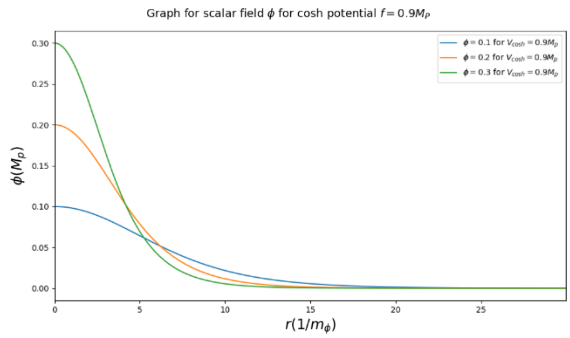

Fig.7: Scalar field for cosh potential at $f\, = 0.9M_p$

Next family of solutions regarding the time and space metric first we will show time metric function in its dimensionless form. As we can see from figures (8-11) at $\tilde{f} = M_p, \Lambda = 0$ as ϕ increase for different potentials the there is a very small change in its configuration because as ϕ increase the mass increase and their radius increase to a certain point where ϕ decrease with mass it will result stability branches.

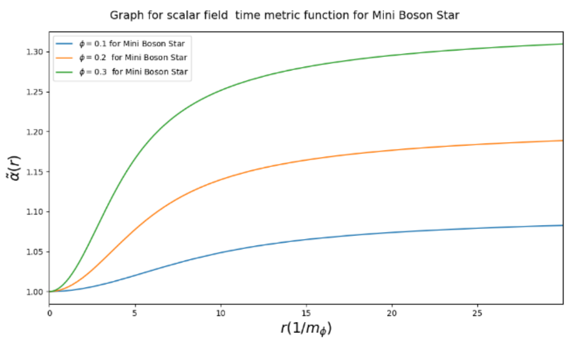

Fig.8: Time metric for mini boson star $\Lambda = 0$

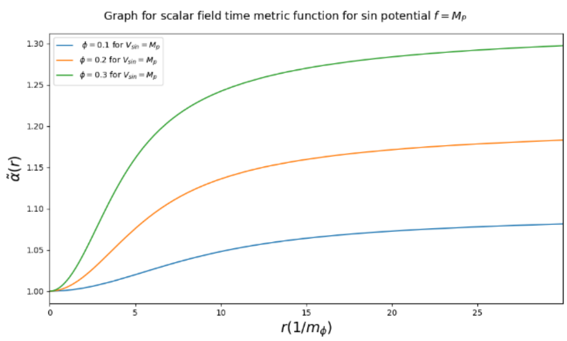

Fig.9: Time metric for sine potential at $f\, = M_p$

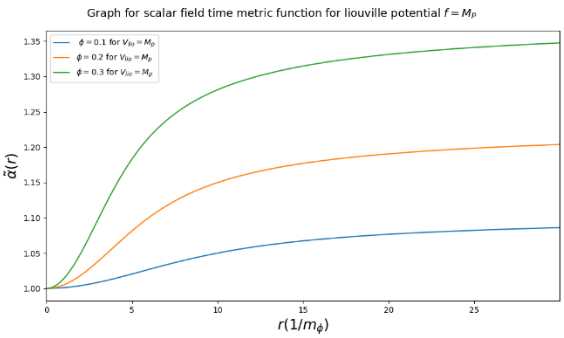

Fig.10: Time metric for Liouville potential at $f = M_p$

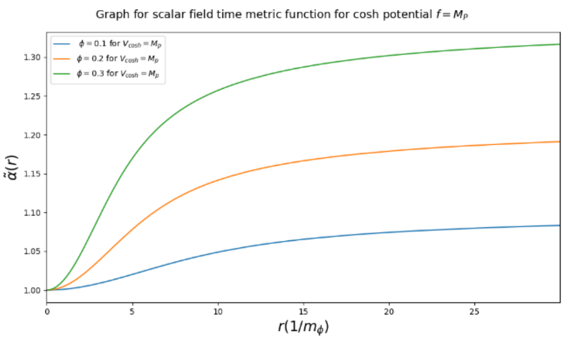

Fig.11: Time metric for cosh potential at $f = M_p$

As we can see from previous figures (12-14) at $\tilde{f} = 0.9M_p$ that as we can the value of decay constant $\tilde{f}$ change slightly to be $\left(0.9M_p\right)$ α as ϕ

increase and due to series forms of U(1) potentials and family of solutions as whole in figures at $\tilde{f} = M_p, \tilde{f} = 0.9M_p$ have very small changes with respect to each ,lastly we have to point out due to equation (7) figures at $\tilde{f} = M_p, \tilde{f} = 0.9M_p$ represent $-\tilde{\alpha}$.

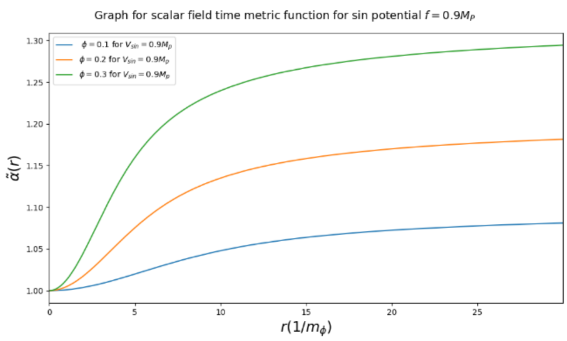

Fig.12: Time metric for Sine potential at $f = 0.9M_p$

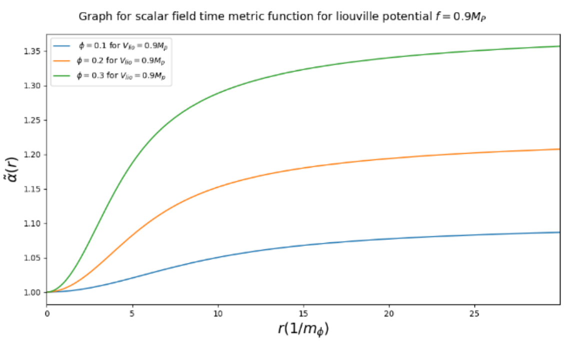

Fig.13: Time metric for Liouville potential at $f = 0.9M_p$

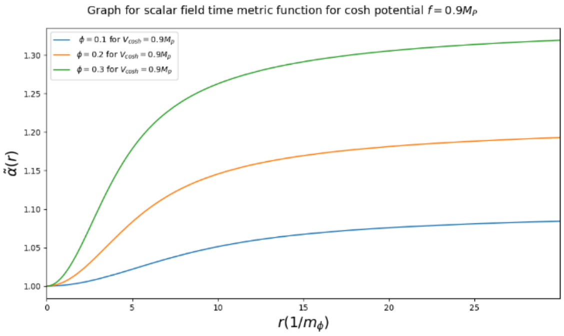

Fig.14: Time metric for cosh potential at $f = 0.9M_p$

Next, we discuss space metric for the same values of ϕ_0 as we did for the time metric. In the figures (15-18), we notice for the space metric at $\tilde{f} = M_p$ and $\Lambda = 0$ that all potentials used have the same peak shape with a very small shift in the peak position towards smaller values of the radial distance r as the value of ϕ_0 increases.

We also observe that the sin potential have slightly lower peaks compared with corresponding cases of the potentials

For the sin potential presented in equation (26) and its series expansion in equation (21), we can see that first two terms represent a quartic potential similar to the one presented in equation (15) but with different numerical values and alternating sign. At the value of $\tilde{f} = M_p$, the series expansion keeps getting smaller till it becomes almost zero which results in lower peaks compared with the other potentials.

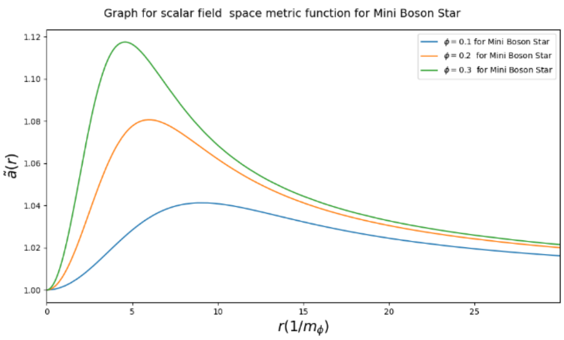

Fig.15: Space metric for mini boson star at $\Lambda = 0$

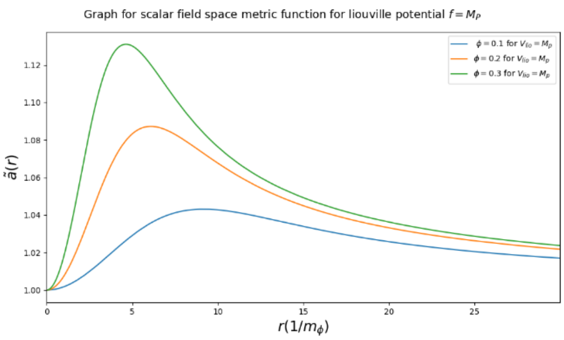

Fig.16: Space metric for Liouville potential at $f = M_p$

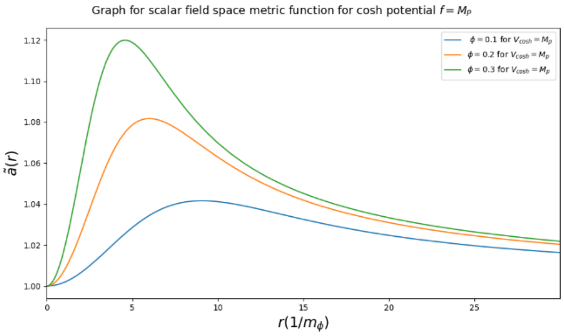

Fig.17: Space metric for cosh potential at $f\ = M_p$

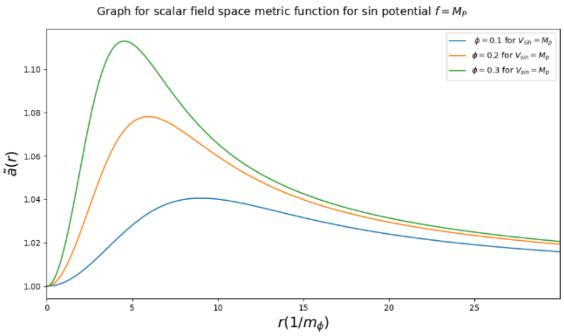

Fig.18: Space metric for Sine potential at $f\ = M_p$

For figures (19-21), we have the same discussion for the case of $\tilde{f}\ = M_p$ presented in the pervious paragraph for the Sin potential, but with the Cosh and Liouville potential have higher peaks at

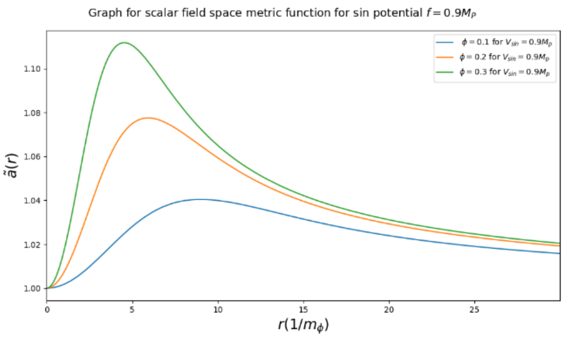

Fig.19: Space metric for sine potential at $f\ = 0.9M_p$

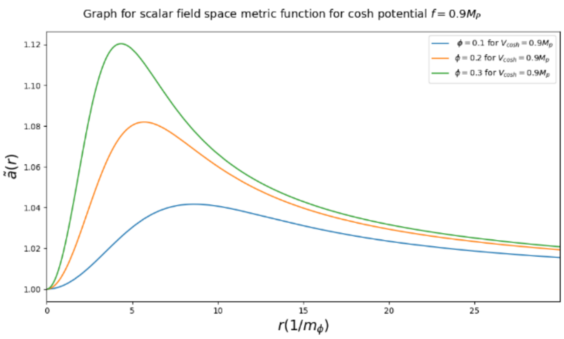

Fig.20: Space metric for cosh potential at $f\ = 0.9M_p$

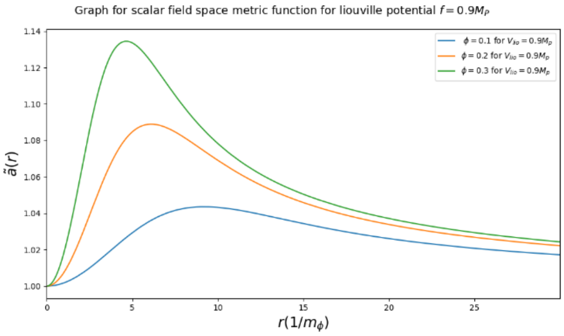

Fig.21: Space metric for Liouville potential at $f = 0.9M_p$

$\tilde{f} = 0.9M_p$ because of the series expansions of these potentials.

In figure (22), we calculated the variation of the mass of the boson star $M(r)$ versus the scalar field ϕ using equation (13) for all the potentials under study. In this figure we included the case of mini-boson star as reference model for the mass to be compared with the other potentials and to check the validity of our numerical code.

Again we use the series expansion in equations (18), (21) and (24) to explain the observed BS mass profile variations at decay constant value $\tilde{f} = 1$. Since we have calculated the mass of the BS using the space and the time metrics, the series expansions of all potentials are expected to have influence on the variation of the mass. This was explained earlier for the case of the sin potential which has a lower maximum mass than the mini BS.

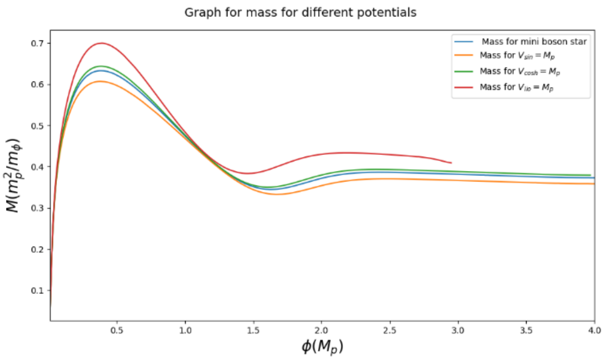

Fig.22: Total star mass with various ϕ *values for different potentials*

On the other hand, the Liouville and cosh potentials are expected to have higher maximum masses than the mini BS.

Next, we provide table (1) below with the calculated maximum mass (M), scalar field (ϕ), and the angular frequency ($\tilde{\omega}$) values. From table (1), the decay constant for the mini-BS ($\Lambda = 0$) and for the rest of potentials at $\tilde{f} = M_p$. Note that all parameters listed in tables (1) and (2) are rescaled. Moreover, from table (1), and as compared with the mini-BS, we observe that BS obtained using Liouville potential has a 9.5% higher maximum mass, while that obtained with the sine potential is (4%), and finally the BS with cosh potential is only (2%) higher.

Potential	$\boldsymbol{\phi(M_p)}$	$\boldsymbol{M(m_p^2/m_\phi)}$	Decay constant	$\boldsymbol{\tilde{\omega}}$
Mini	0.38	0.633	0	1.241
Cosh	0.38	0.643	M_p	1.247
Sin	0.38	0.606	M_p	1.226
Liouville	0.39	0.699	M_p	1.293

Table 1: Comparison of different potential forms used and their corresponding maximum mass at decay constant $\tilde{f} = M_p$.

Lastly, we are going to repeat the same procedure described above but for another value of the decay constant; $\tilde{f} = 0.9M_p$.

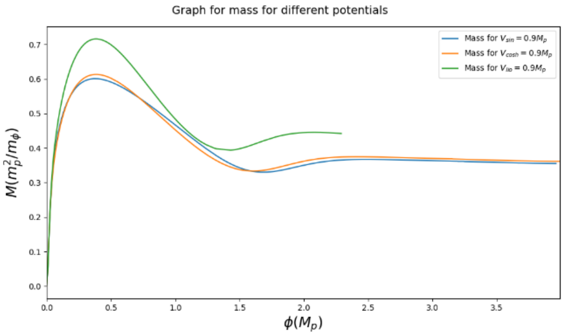

Fig.23: Maximum mass for U(1) potential at $\tilde{f} = 0.9M_p$

As we can see from figure (23), and as compared to the $\tilde{f} = M_p$ case, the maximum mass for the cases of the cosh and the sine potentials are significantly closer to each other, and even share almost the same maximum mass for the same scalar field. More interestingly, the case of Liouville potential at $\tilde{f} = 0.9M_p$ shows a higher maximum mass than both the Cosh and Sin potentials with same decay constant. This is expected to yield a comparatively higher compactness for the case of Liouville potential which may be a suitable model to study dark matter candidates and also gravitational waves resulting from compact star collapse at much smaller values of the decay constant. The above-mentioned observation is left for a future study.

Potential	$\boldsymbol{\phi(M_p)}$	$\boldsymbol{M(m_p^2/m_\phi)}$	Decay constant	$\tilde{\boldsymbol{\omega}}$
Cosh	0.39	0.613	$0.9M_p$	1.326
Sin	0.38	0.600	$0.9M_p$	1.223
Liouville	0.39	0.715	$0.9M_p$	1.305

Table 2: Comparison of potential forms and their maximum mass at decay constant $\tilde{f} = 0.9M_p$

From Table (2), we observe that as compared with the mini-BS, the BS obtained using the cosh potential has a maximum mass that is lower by (3%) and BS obtained using the sine potential is almost (5%) lower. On the other hand, in this configuration the BS obtained using the Liouville potential has the highest maximum mass which is (11.5%) higher than the that for the mini-BS.

In the next section, we will discuss the implications of the maximum mass data presented above in the context of the study of black hole mimicking.

3. Accretion disc model and power spectrum

In this section, we adopt the same procedures as in references [7] and [21] to calculate the power-spectrum of the compact objects being compared using the disc model. Using the spherically symmetric line element mentioned above in equation (7), we calculate the time-like geodesic.

$$\dot{r}^2 + \frac{1}{a^2}\left(1 + \frac{L^2}{r^2}\right) = \frac{E}{\alpha^2 a^2}\,, \qquad (29)$$

where $L^2 = r^4\dot{\varphi}^2$ is the squared angular momentum, $E^2 = -\alpha^2\dot{t}^2$ is the squared total energy at spatial infinity, φ is the azimuthal angle, and t is time. The dot over the components the right-hand side of the L^2 and E^2 represent the proper time derivative for the test particle.

The study of stable orbits of a test particle demands the following identification in equation (29)

$$V_{effective}^2 = \frac{1}{\alpha^2}\left(1 + \frac{L^2}{r^2}\right), \qquad (30)$$

where $V_{effective}^2$ is an effective potential. For a test particle we only consider circular orbits with $\dot{r} = 0$ then the potential becomes

$$V = \left(\left(1 + \frac{L^2}{r^2}\right) - \frac{E^2}{\alpha^2}\right)/\alpha^2. \qquad (31)$$

Solving (31) under the conditions of circular orbits, that is $\dot{r}$ and $\frac{dV}{dr} = 0$, we get the following equations for energy, angular momentum angular velocity, respectively:

$$E = \frac{\alpha^2}{\sqrt{\alpha^2 - r\alpha\alpha'}}, \qquad (32)$$

$$L = \sqrt{\frac{r^3\alpha\alpha'}{\alpha^2 - r\alpha\alpha'}} \qquad (33)$$

, and

$$\Omega = \sqrt{\frac{\alpha\alpha'}{r}} \qquad (34)$$

Then for accretion disc, we demand it to be steady, geometrically thin and optically thick

$$D(r) = \frac{\dot{M}}{4\pi r}\frac{\alpha}{a}\left(-\frac{d\Omega}{dr}\right)\left(\frac{1}{(E - \Omega L)^2}\right)\int_{r_i}^{r_f}(E - \Omega L)\frac{dL}{dr}dr \qquad (35)$$

Where $\dot{M}$ is accretion disc rate, r_i is inner disc edge and r_f is outer edge of disc note we choose disc inner disc edge to be zero for boson star since it allows circular orbits in all spatial domain and also it does not affect disc as long it is made of test particles. Lastly, the outer edge we demand to be at innermost stable circular orbit (ISCO) $r_f = 6M$.

We assume the accretion disc to have local temperature defined by Stefan-Boltzmann law $D(r) = \sigma T^4$, where σ is Stefan-Boltzmann constant. We can consider our disc to emit radiation as a black body then luminosity can be expressed by the form

$$L(v) = \frac{16\pi h}{c^2}\cos(\theta)\, v^3 \int_{r_i}^{r_{max}} \frac{r dr}{e^{\frac{hv}{kT}} - 1} \qquad (36)$$

, where h is Planck constant, c is speed of light k is Boltzmann constant v is frequency and θ is disc inclination.

3.1. Results and discussion

In this section, we are going to find the luminosity for different sets of BSs and BHs with different potentials that are discussed earlier in section (2).

First, we display the luminosity for BSs and BHs at maximum mass using equation (36). The corresponding results are depicted in figures from (24) to (30).

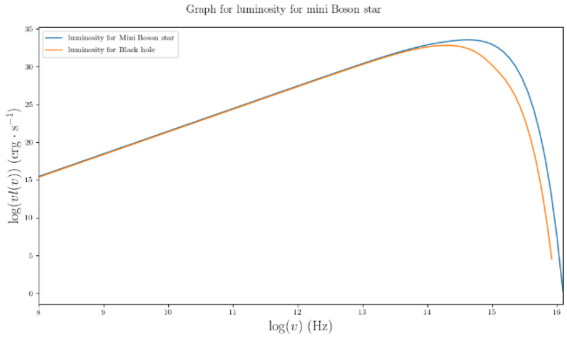

Fig.24: luminosity at maximum mass for Mini Boson star

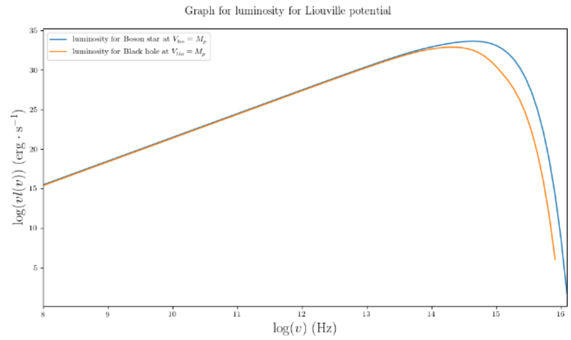

Fig.25: luminosity at maximum mass for Liouville potential Boson star at $f = M_p$

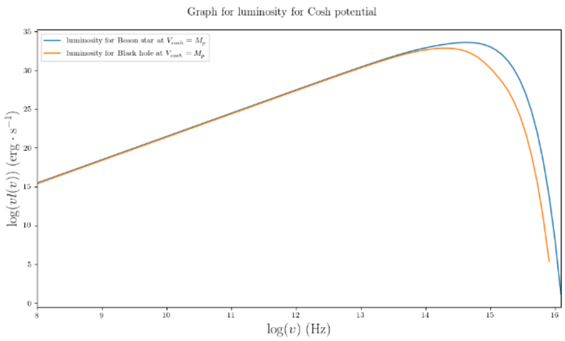

Fig.26: luminosity at maximum mass for cosh potential Boson star at $f = M_p$

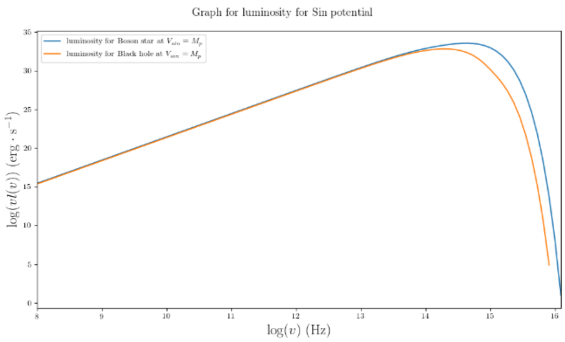

Fig.27: luminosity at maximum mass for sine potential Boson star at $f = M_p$

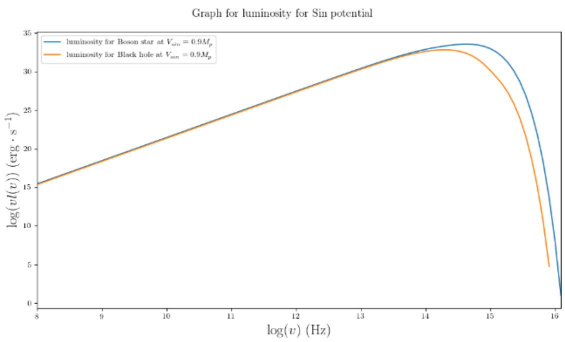

Fig.28: luminosity at maximum mass for sine potential Boson star at $f = 0.9M_p$

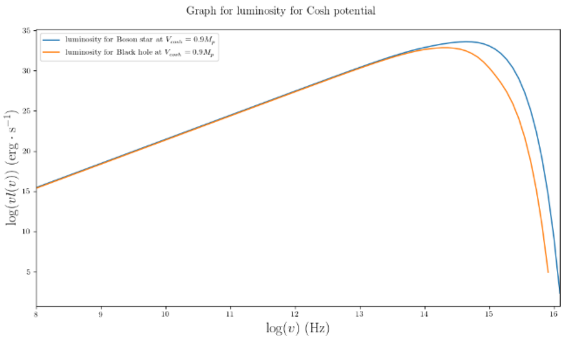

Fig.29: luminosity at maximum mass for cosh potential Boson star at $f = 0.9M_p$

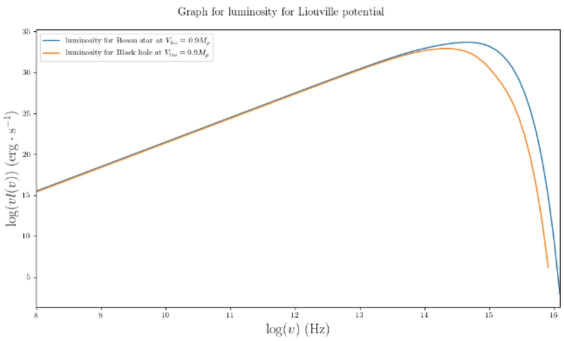

Fig.30: luminosity at maximum mass for Liouville potential Boson star at $f = 0.9M_p$

Potential	$\boldsymbol{\phi(M_p)}$	Star mass $\boldsymbol{M(m_p^2/m_\phi)}$	Boson star scalar field mass m[GeV]	Black hole mimicker $\boldsymbol{m_{BH} = [Gev]}$
Mini	0.18	0.503	2.8×10^{-29}	2.22×10^{-29}
Cosh	0.18	0.576	2.85×10^{-29}	2.5×10^{-29}
Sin	0.18	0.6322	2.68×10^{-29}	2.8×10^{-29}
Liouville	0.19	0.522	3.01×10^{-29}	2.3×10^{-29}

Table 3: Values of Black hole mimickers for different potentials

Before getting deeper in our discussion, we prefer to introduce our method of calculation.

First, we compute the BH time and space metrics using the equation $\alpha^2 = 1/a^2 = (1 - 2M(r)/r)$. Then we calculate the components of the disc model for both BHs and BSs. By ‘components’, here, we mean energy, angular momentum and angular velocity given in equations (32-34), which are necessary to calculate the luminosity in equation (36).

For both cases we use BH by mass $\left(3 \times 10^{9} M_{\odot}\right)$ and accretion rate $\left(\dot{M} = 3 \times 10^{-6} M_{\odot}/yr\right)$. Note that our chosen disc angle has in equation (35) $\theta = 60°$. We also choose a BH configuration for which we assume an inner radius at ISCO = $6M(r)$. Lastly, we assume that the outer disc is at $50M(r)$, where $M(r)$ is already defined in equation (13).

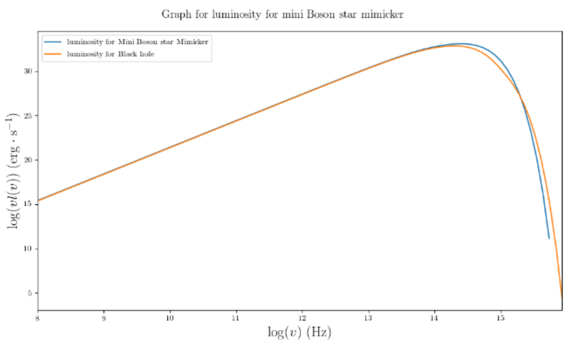

Fig.31: luminosity for a black hole at maximum mass and its mini-boson star mimicker

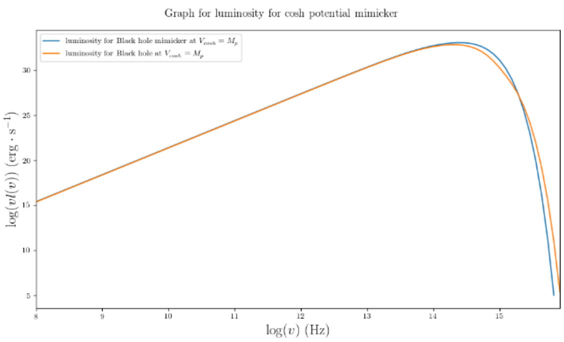

Fig.32: luminosity for a black hole at maximum mass and its cosh boson star mimicker

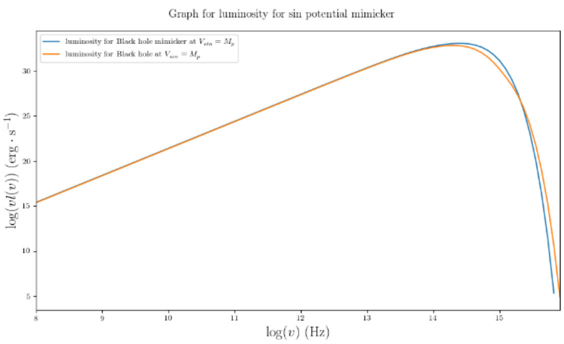

Fig.33: luminosity for a black hole at maximum mass and its Sine boson star mimicker

Now we use the maximum mass data listed in tables (1) and (2) which corresponds to the potentials under study. We use the maximum mass because it represents the most compact configuration of the BS. Then we search to find its black hole mimicker, which is some BS configuration in the present study.

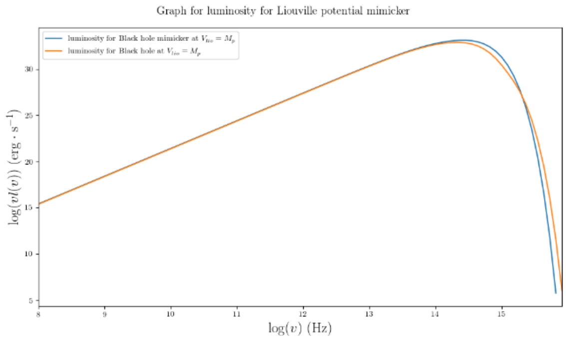

Fig.34: luminosity for a black hole at maximum mass and its Liouville boson star mimicker

Now we present a family of solutions for equation (36) at several frequencies v. Here we have used the maximum mass data from table (1). We present BSs and BHs (at maximum mass) luminosity curves depicted in figures from (31) through (34). These family of solutions are calculated at $(\Lambda = 0, \tilde{f} = M_p)$. In these figures we searched for BS by changing scalar field ϕ_0 that can mimic BH at maximum mass until they all have almost the same behaviour. In this endeavour, we use the parametric relation $m[GeV] = 1.33 \times 10^{-25} \frac{M(\infty)}{M_{BH}}$ introduced in reference [22] to calculate scalar field mass. Note that $M(\infty)$ is the rescaled value of mass calculated at the very far outer boundary of star and M_{BH} is the corresponding BH mass. Then we search for a BS mimicker to the BH at maximum mass for each configuration presented in the table (3). From these values of the scalar field mass obtained for BS configurations corresponding to different potentials, we can see that the scalar field values that produce BH mimickers are all in the order of (10^{-29}) GeV. Based on the above mentioned parametrization, this is because of the BH mass used is $3 \times 10^9 M_\odot$.

Table 4. Values of black hole mimickers for different potentials at $\tilde{f} = 0.9M_p$

Potential	$\phi(M_p)$	Star mass $M(m_p^2/m_\phi)$	Boson star scalar field mass m[GeV]	Black hole mimicker $m_{BH} = [Gev]$
Cosh	0.18	0.548	2.71×10^{-29}	2.43×10^{-29}
Sin	0.18	0.548	2.66×10^{-29}	2.43×10^{-29}
Liouville	0.221	0.661	3.16×10^{-29}	2.9×10^{-29}

Table (4) depicts the BH maximum mass data but for $\tilde{f} = 0.9M_p$. As we can see from the mimicker solution family from table (4) and figures that figures (35-37) in all are all most identical. We expect the same behaviour to persist up to $\tilde{f} = 0.1M_p$.

For $\tilde{f}$ values lower than $0.1M_p$, further studies are needed, especially for the configurations involving Liouville and sin potentials. We can see for tables (3) and (4) that the BH mimicker obtained using Liouville and cosh potentials can be used to investigate the upper bound of the scalar field mass at low $\tilde{f}$. The maximum star mass obtained is proportional to $\tilde{f}$.

Based on the above mentioned parametric equation, we expect that for the scalar field mass near ~ GeV scale, the corresponding black hole mimicker mass should be ~ 10^{-20}M$_\odot$, which is theorized in the models of the very early universe incorporating primordial black holes [25]. Thus, we anticipate that the scalar field for a bosonic BH mimicker could be axions, which we plan to investigate in a future study.

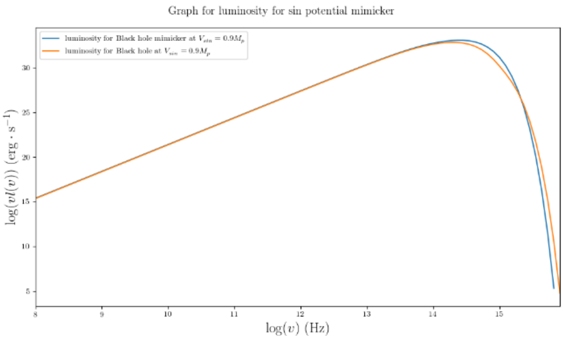

Fig.35. luminosity for a black hole at maximum mass and its sine boson star mimicker at $f = 0.9M_p$

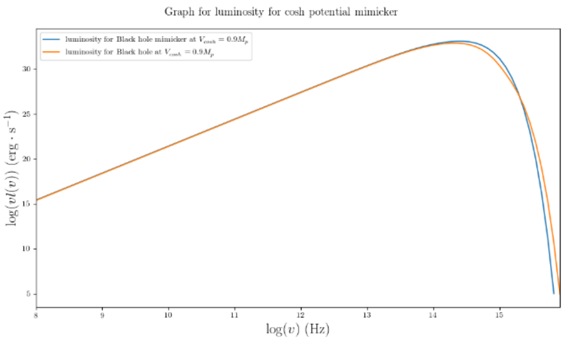

Fig. 36. luminosity for a black hole at maximum mass and its cosh boson star mimicker at $f = 0.9M_p$

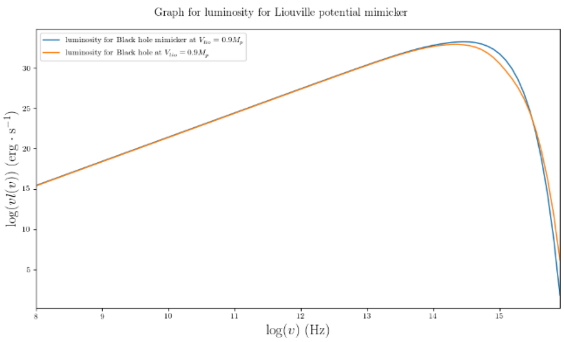

Fig. 37. luminosity for a black hole at maximum mass and its Liouville boson star mimicker at $f = 0.9M_p$

3.2. Observational challenges

The two main distinctions between a black hole and a boson star are that the former has a singularity, while the latter does not have an event horizon. In certain situations, this distinction may be difficult to observe, although hints would be provided by the absence of an event horizon, shadow features, and gravitational wave signal. As our observational capabilities advance, particularly in direct imaging and gravitational wave astronomy, these distinctions will become more apparent.

If we want to observe a boson star configuration, we need to fix either the mass or the radius of the star. Determining the mass of a boson star helps make its observational characteristics more predictable and facilitates distinguishing it from other cosmic objects. This improves the likelihood of detecting or confirming its existence using different observational methods. If you detect an object with a mass between $10^2\,M_\odot$ and $10^5\,M_\odot$, it could be either a boson star or a black hole. However, if the mass surpasses $10^5\,M_\odot$, it is more likely to be a black hole, as boson stars typically cannot attain such a large mass. In terms of orbital dynamics, if you observe orbital behaviour around the object and detect weaker, more spread-out gravitational effects than expected from a black hole, this may indicate a boson star, especially if the mass is on the lower to mid-range. In contrast, a black hole usually causes rapid acceleration of objects toward a dense singularity. As for the event horizon and singularity, if you have access to high-resolution imaging, such as from the Event Horizon Telescope, and can observe a "shadow" or a region of darkness at the centre of the object, it's likely a black hole. On the other hand, a boson star, which doesn't have an event horizon, may show a more diffuse boundary, and you might observe material flowing or moving in a way that indicates the absence of a distinct boundary. Moreover, if gravitational waves are detected, their waveform will offer crucial information. The "ringdown" phase—unique to black hole mergers—will not be present in mergers of boson stars, as they lack the event horizon. Finally, in terms of light and radiation emission, If you detect an X-ray or gamma-ray source emitting substantial radiation from a small region with no visible light source (indicating a black hole), this points to the presence of a black hole. However, the absence of a distinct event horizon, coupled with intense radiation, could indicate a boson star.

The maximum mass can be controlled by the decay constant f, which by turn is controlled by the self-interaction Λ. A smaller decay constant typically corresponds to a larger maximum mass for the star. If gravitational wave signals are considered for BS detection, a larger decay constant (weaker interactions) might lead to less compact boson stars, producing a different gravitational waveform than more strongly interacting (smaller decay constant) stars. By examining the frequency, amplitude, and shape of the detected gravitational waves, it is possible to deduce the characteristics of the object that produced them, such as the decay constant through the star's self-interaction strength.

To determine the decay constant, the observed gravitational waveform is compared with theoretical models of boson stars featuring varying decay constants. By aligning the theoretical models with the observed waveform, the decay constant that best matches the data can be identified. This process usually involves parameter estimation, where the model parameters, including the decay constant, are refined to reduce the discrepancy between the predicted and observed waveforms.

4. Summary and Conclusion

In the present paper, we introduced spherically symmetric boson stars as potential black hole mimickers, We used the power spectrum from a typical thin, steady-state, geometrically thin disc, similar to the standard model for astrophysical black holes. However, we adapted the disc model for the specific properties of boson stars. We used the line element and Lagrangian adopted by the authors of ref. [7], then we extrapolated the calculations to a variety of other U(1) potentials beyond that in this reference. Our present work can be divided into the following steps:

- Producing Boson star system of equations using ADM formalism of numerical relativity.
- Rescaling this system of equations to be dimensionless making the numerical system more balanced. This can help prevent instability caused by very large or very small numbers.
- Introducing U(1) potentials in their original form then modifying them to include only a one decay constant term.
- Rescaling these potentials to be dimensionless.
- Presenting the key parameters of the BS system such as the characteristic size, metric functions, central scalar field amplitude, and maximum mass.
- Discussing accretion disc model and power spectrum for different potentials and finding black hole mimickers for these potentials at maximum mass.

In our calculations, we computed numerical solution to our ordinary differential equation with arbitrary value $\tilde{\omega}$ with the main feature that as system of equations (10a–10d) tends to infinity system grow exponentially, we performed binary search for this unknown value of $\tilde{\omega}$ in the range $[\widetilde{\omega_i}, \widetilde{\omega_f}]$ using our code, which we coded from scratch, to ensure that we have unique value for $\tilde{\omega}$ that exists in this range for each value of $\tilde{\phi}$. The solutions must not have any nodes or zeros to make sure we describe the ground state of the BS but not the excited states, which is out of scope of this paper.

In this work we shed light on U(1) potentials with higher order terms than that presented in [18] to see how BS system will differ accordingly in its maximum mass from one type of potential to another. As depicted in Table (1), we primarily found that Liouville-type potential will yield slightly (9.5%) higher maximum mass as compared with the mini-boson star model.

Furthermore, as the decay constant decreases below Planck mass it will result in even higher value of maximum mass and also a higher compactness as presented in Table (2). In the rest of this work, we discussed simple compact object disc model and power spectrum to find out if these potentials will give rise to an “observable” distinct behaviour in its power spectrum.

Our arguments lied down section (3.1) based upon the parametric equation correlating the scalar field mass with the maximum BS star mass suggest that if one plans to model a black hole mimicker corresponding a given black hole mass such that the BS is composed of scalar fields that are comparable in mass with, for example, the theorized early universe's QCD axions, it'd be more convenient to assume scalar-field self-interactions of the Sin-Gordon type, that is the type corresponding to the comparatively lowest maximum BS mass.

Further studies need to be made on these BS configurations at values of decay constant lower than $f = 0.9M_p$. As detailed in section (3.2), small values of the decay constant can lead to an increase in the maximum mass of the boson star. This fact gives a generous opportunity for suggesting empirical scenarios not only to probe BSs but also to differentiate between a Black Hole and its BS mimicker. The observation facilities to differentiate BHs from BSs include:

- Gravitational wave astronomy; wave form analysis and parameter estimation.
- Electromagnetic observations; light curves, spectra, and X-ray emissions.
- Direct imaging via the Event Horizon Telescope.

Possible extension of this work include but not limited to study dynamic boson star configurations at lower decay constants, study of the perturbations during possible decay scenarios of boson star mimickers as a signature for gravitational waves.

Acknowledgments

Not available.

Funding statement

This study didn't receive any funding support.

Declaration of Conflict of Interest

The authors declare that there is no conflict of interest.

Ethical approval

This study follows the ethics guidelines of the Faculty of Science, Helwan University, Egypt (ethics approval number: REC-Sci-HU/P35-10-02.

References

[1] T. W. Baumgarte and S. L. Shapiro. Numerical relativity: starting from scratch. Cambridge University Press, 2021.

[2] G. Choi, H. He, and E. D. Schiappacasse. Probing dynamics of boson stars by fast radio bursts and gravitational wave detection. Journal of Cosmology and Astroparticle Physics, 2019(10):043, 2019.

[3] M. Colpi, S. L. Shapiro, and I. Wasserman. Boson stars: Gravitational equilibria of self-interacting scalar fields. Physical review letters, 57(20):2485, 1986.

[4] D. Croon, J. Fan, and C. Sun. Boson star from repulsive light scalars and gravitational waves. Journal of Cosmology and Astro particle Physics, 2019(04):008, 2019.

[5] M. Gleiser. Stability of boson stars. Physical Review D, 38(8):2376, 1988.

[6] M. Gleiser and R. Watkins. Gravitational stability of scalar matter. Nuclear Physics B, 319(3):733–746, 1989.

[7] F. S. Guzmán and J. M. Rueda-Becerril. Spherical boson stars as black hole mimickers. Physical Review D—Particles, Fields, Gravitation, and Cosmology, 80(8):084023, 2009.

[8] S. H. Hawley and M. W. Choptuik. Boson stars driven to the brink of black hole formation. Physical Review D, 62(10):104024, 2000.

[9] J. Ho, S. Kim, and B-H Lee. Maximum mass of boson star formed by self-interacting scalar fields. arXiv preprint gr-qc/9902040, 1999.

[10] K. Iwasawa and G. Miniutti. Broad iron lines in AGN: The case of mcg–6-30-15. Progress of Theoretical Physics Supplement, 155:247–258, 2004.

[11] D. J. Kaup. Klein-Gordon geon. Physical Review, 172(5):1331, 1968.

[12] F. V. Kusmartsev, E. W. Mielke, and F. E Schunck. Gravitational stability of boson stars. Physical Review D, 43(12):3895, 1991.

[13] C-W Lai. A numerical study of boson stars. arXiv preprint gr-qc/0410040, 2004.

[14] E. W. Mielke and Reinhard Scherzer. Geon-type solutions of the nonlinear Heisenberg-Klein-Gordon equation. Physical Review D, 24(8):2111, 1981.

[15] E. A. Power and J. A. Wheeler. Thermal geons. Reviews of Modern Physics, 29(3):480, 1957.

[16] R. Ruffini and S. Bonazzola. Systems of self-gravitating particles in general relativity and the concept of an equation of state. Physical Review, 187(5):1767, 1969.

[17] F. E. Schunck and A. R. Liddle. The gravitational redshift of boson stars. Physics Letters B, 404(1-2):25–32, 1997.

[18] F. E. Schunck and D. F. Torres. Boson stars with generic self-interactions. International Journal of Modern Physics D, 9(05):601–618, 2000.

[19] E. Seidel and W-M Suen. Dynamical evolution of boson stars: Perturbing the ground state. Physical Review D, 42(2):384, 1990.

[20] P. Slany and Z. Stuchlik. Mass estimate of the XTE j1650-500 black hole from the extended orbital resonance model for high-frequency QPOs. Astronomy & Astrophysics, 492(2):319–322, 2008.

[21] D. F. Torres. Accretion disc onto a static non-baryonic compact object. Nuclear Physics B, 626(1-2):377–394, 2002.

[22] D. F. Torres, S. Capozziello, and G. Lambiase. Supermassive boson star at the galactic centre? Physical Review D, 62(10):104012, 2000.

[23] J. A. Wheeler. Geons. phys. Rev, 97:511–36, 1955.

[24] S. L. Liebling, C. Palenzuela. Dynamical boson stars. Living Reviews in Relativity. 2023 Feb 24; 26(1):1.

[25] D. J. E. Marsh. Axion Cosmology. Physics Reports. 2016; 643: 1-79.

[26] G. M. Bower, D. A. Kormendy, and J. H. Ho, "Supermassive black holes in active galactic nuclei," *Annu. Rev. Astron. Astrophys.*, vol. 46, pp. 485-514, 2008.

نجوم البوزون ذات الجهود المتماثلة من النوع U(1) كمرشحين لمحاكاة الثقوب السوداء

الملخص

نحن ندرس تكوين نموذج نجم بوزوني متماثل كرويًا مع شروط التفاعل الذاتي العامة من نوع التناظر U(1). نقوم بتعديل هذه الجهود لتشمل ثابت اضمحلال واحد فقط مما يؤدي إلى تغيير بسيط في تكوين كتلة النجم. نحن ندرس هذه التشكيلات بدلالة نموذج قرص التراكم البسيط حول النجم البوزوني. لقد وجدنا تكوينًا فريدًا لنجم بوزوني يحاكي تكوينًا معينًا للثقب الأسود وذلك من خلال دراسة طيف الطاقة عند قيم مختلفة لثوابت الاضمحلال لتشكيلات من النجوم البوزونية المختلفة التي تمت دراستها. أخيرًا، وضعنا مخططًا لمطابقة إشارات الموجات الثقالية التي تم رصدها حاليًا مع الحد الأقصى لكتل محاكيات النجم البوزوني التي حصلنا عليها كنواة لبحث قادم.

الكلمات الدالة: نجوم البوزون، النجوم المضغوطة، الثقوب السوداء، النسبية العامة، المجالات العددية، معادلات أينشتين-كلاين-جوردون.